Available online at www.sciencedirect.com

ScienceDirect

journal homepage: www.elsevier.com/locate/he

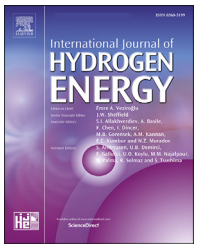

# Thermally annealed self-assembled three-dimensional graphene for direct construction of porous flow distributor in polymer electrolyte membrane fuel cell

*Gil Won Lee* [a,1], *Changwook Seol* [a,1], *Koung Moon Kim* [a], *Sun Taek Lim* [a], *Gyu Hyeon Shim* [a], *Sang Moon Kim* [a,*], *Ho Seon Ahn* [a,b,**]

[a] *Department of Mechanical Engineering, Incheon National University, Incheon, 22012, Republic of Korea*
[b] *AHN Materials Inc., Incheon, 21990, Republic of Korea*

## HIGHLIGHTS

- The conductivity of STG flow distributor is improved via thermal annealing process.
- Advanced STG flow distributor leads to the enhanced performance of PEMFC system.
- Thermal annealing to STG is effective for lowering ohmic & kinetic resistances.
- Advanced STG shows remarkable potential for replacing CVD-based 3D graphene.

## ARTICLE INFO

*Article history:*
Received 20 April 2021
Received in revised form
25 August 2021
Accepted 30 August 2021
Available online 25 September 2021

*Keywords:*
PEMFC
Porous flow distributor
3D graphene
Thermal annealing
Advanced boiling method

## ABSTRACT

Self-assembled three-dimensional graphene (STG), which is constructed via advanced boiling method (ABM) has advantages in terms of low-cost, facile procedures, and needless to use any backbone structure. Although the previously developed STG is considered as a promising material and structure to be used as a flow distributor in polymer electrolyte membrane fuel cell (PEMFC), the STG flow distributor should be advanced in the aspect of conductivity to achieve higher performance. Herein, the conductivity of STG is improved via the thermal annealing process and the advanced STG is applied in PEMFC as a flow distributor to enhance the performance of the single-cell system. Single cell constructed with the thermally annealed STG exhibits a lowered charge and ohmic resistance, which leads to the performance enhancement. These results imply that direct coating of the advanced STG can be one of the alternatives of the complex and high-cost process of graphene coating to the porous metal foam through chemical vapor deposition (CVD).



* *Corresponding author.*
** *Corresponding author.* Department of Mechanical Engineering, Incheon National University, Incheon, 22012, Republic of Korea.
E-mail addresses: ksm7852@inu.ac.kr (S.M. Kim), hsahn@inu.ac.kr (H.S. Ahn).
[1] These authors equally contribute to this manuscript.

https://doi.org/10.1016/j.ijhydene.2021.08.210

## Introduction

As the fuel cell is considered a promising future green technology, polymer electrolyte membrane fuel cells (PEMFCs) have attracted much attention due to eco-friendliness, low operating temperature, short start-up time, and high efficiency. The PEMFC system consists of the membrane electrolyte assembly (MEA), gas diffusion layers (GDLs), end-plate, and bipolar plates. Among the components of the single PEMFC system, the bipolar plates are regarded as one of the essential parts of the system, since the bipolar plates act as an electron pathway because the electron could not directly move through the MEA, and it supports MEA physically at the assembled fuel cell system. Furthermore, one of the indispensable roles of the bipolar plate is supplying reactant and removing the generated water from the MEA through its own flow distributor. It is widely known that the water management and uniform reactant gas supply in the fuel cell system is one of the significant factors which determines the single cell performance. Hence, the various designs of flow distributor have been investigated for facilitating mass transport and reducing pressure drop in the channel. Among many types of flow distributor, the serpentine channel flow distributor has been widely used in fuel cell systems due to the fact that this configuration is effective for removing water. However, the serpentine-shaped channel has disadvantages in the aspect of comparatively severe pressure drop and inferior gas supply from the channel to the catalyst layer at the rib where the bipolar plate and GDL contact. To address these issues, the porous flow distributor, which is advantageous for facilitating uniform gas supply over the active area, was suggested. After the conceptual design of the porous flow distributor was suggested in US patent, numerous follow-up studies have exhibited the effectiveness of the porous distributor on enhancing PEMFC performance [1]. First, A. Kumar and R.G. Reddy had experimentally used Ni–Cr foam as a flow distributor, which leads to enhanced performance compared to the fuel cell with conventional flow distributor [2]. After then, many following studies reported more enhanced PEMFC performance through applying the modified porous flow distributor [2–8]. In the aspect of material of the porous flow distributor, most of the studies have generally used Ni-based metal foams, which have corrosion issue in the acidic condition and MEA poisoning issue due to the ionized metal [9–13]. Hence, some researchers have studied porous 3D graphene materials, which withstand high chemical stress, to address critical corrosion and MEA poisoning issues [4–6]. Graphene, as one of the materials in the spotlight, is considered superlative materials due to its outstanding properties of electrical/thermal conductivity, stiffness, and, mechanical strength [14–19]. Due to the superior properties, graphene materials have been applied to metallic flow distributor to enhance electrical/thermal conductivity or corrosion resistance [4–6,20–23]. And mostly, coating graphene onto the bipolar plates (flow distributor) has been conducted through chemical vapor deposition (CVD) method. Even though the CVD process is advantageous to achieve a uniform and high-quality coating of the graphenes, the process requires extremely high temperature (~1000 °C) and post etching process of the 3D matrix substrates, such as Ni foam [24,25]. For these restrictions, the development of a facile and simple method to construct 3D graphene structures is needed. That is why the direct 3D structuring of chemically exfoliated graphene has recently received attention as the advanced methods to obtain a chemically stable 3D porous flow distributor. In our previous study, we have constructed the self-assembly three-dimensional graphene (STG) via advanced boiling method (ABM), also known as super-heated vaporization of micro-droplet method. The STG was directly constructed on the bipolar plates to act as a flow distributor in the single cell system [26]. Due to the fact that ABM does not require the backbone structure or extremely high-temperature condition, it is a cost-saving process in comparison with the conventional CVD method, apparently. Although the STG flow distributor exhibited sufficient potential to be applied in PEMFC system with advantages of direct 3D structuring via facile spray process, the single-cell performance with STG flow distributor did not reach that of conventional flow distributor. This result implies STG flow distributor should be more improved to be a strong alternative for conventional porous flow distributors. Since STG is constructed using the reduced graphene oxide (rGO), STG has some drawbacks, including lowered electrical conductivity during the oxidation process [27–29]. Thus, a further process should be considered for recovering the degraded conductivity of STG. After Gao et al. reported that chemically exfoliated graphene could be further reduced by decomposing oxygen-containing functionalities via thermal annealing process, it is regarded as the assuring technique to recover the properties of rGO [30,31]. In this study, with the thermal annealing process, the recovered electrical/thermal conductivity of STG can be obtained, which could enhance the single-cell performance. Hence, the thermal annealing process of constructed STG flow distributor was carried out with a variation of annealing temperature. In addition, to elucidate the effect of the annealing on PEMFC performance enhancements, STG flow distributor and bipolar plate are characterized and analyzed via thermal gravimetric analysis (TGA), scanning electron microscopy (SEM), contact angle measurements, electrochemical impedance spectroscopy (EIS), X-ray photoelectron spectroscopy (XPS), and optical microscopy.

## Experimental section

### *Preparation of rGO colloid*

Chemically exfoliated graphene was synthesized via the improved Hummer's method, which includes the chemical oxidation of graphite and sonication procedures [32]. 40 ml of phosphoric acid (Daejung, 85%) and graphite powder 3 g (Sigma-Aldrich, 325 mesh) were dispersed into the 360 ml of sulfuric acid (Daejung, 95%). Then, potassium permanganate 18 g (Daejung, 99%) was slowly added to the acidic graphite mixture. It is noted that the mixture was stirred and kept in a heating jacket at 50 °C for 22 h. After the treatment, 400 ml of distilled water and 3 ml hydrogen peroxide (Daejung, 30%) were added into the mixture. And the mixture was vacuum-filtrated to dehydrate. After the vacuum filtration process, the graphite oxide (GO) cake was dispersed in chloric acid

(Samchun, 35%) and mixed with distilled water for the rinsing process. And then, a centrifuge process was carried out to remove impurities for 30 min at 4000 rpm. After centrifugation, the GO cake was vacuum filtrated once more to remove further impurities that may have remained. After the 2nd vacuum filtration process, the GO cake was freeze-dried to fully dehydrate at −100 °C for 4 days in a freeze-dryer. After that, the fully dried GO cake was pounded to turn into powder. The SEM images of fully dried GO cake and the GO powder can be founded in Fig. S1. This synthesized GO powder was dispersed in 500 ml of distilled water to obtain density of 1 mg/ml. This GO colloid was ultrasonicated to exfoliate the graphene sheets at 60% amplitude of the sonicator for 40 min (Sonics Vibra-Cell VC 505, 500 W). The brown-colored graphene oxide colloids after ultrasonication process were reduced at 90 °C for 1 h with 1750 μl of ammonia (Samchun, 25–30%) and hydrazine solution 1000 μl (Sigma-Aldrich, 35%). The detailed information such as chemical composition of synthesized rGO solution can be founded in our previous study [33].

### *Construction of optimized STG flow distributor via ABM*

The ABM was applied to construct STG flow distributor directly on the cathode bipolar plate, which was made of SUS316L. It is noted that constructing 3D porous graphene material via ABM has advantages as follows: low-cost, time-saving, and low-temperature condition. Furthermore, it does not require any backbone structure, which means further etching process does not require compared to CVD method for graphene coating on 3D porous backbone [33]. After the micro-droplets are discharged to the bipolar plate, they are superheated and vaporized rapidly due to the heat of the target surface (200 °C). The dispersed rGO sheets in the micro-droplets form an inhomogeneous residue after the complete vaporization of micro-droplets. As the spray process is repeated, these residue rGO sheets are assembled at the complex interface (triple point), constructing a porous network resembling the shape of vaporized micro-droplets, which act as a seed for constructing STG. In order to control the spray discharging process, the relay module was controlled via our research group's own house code. To prevent over-cooling/heating of the heating block during the STG construction process, the cartridge heater, which is inserted in the heating block, is controlled via PID control. The spray delay time was set to be 25 s to maintain steady-state temperature conditions, and the micro-droplets of rGO colloid discharging time was set to be 1 s. When the charging-discharging cycle was repeated 150 times, STG is fabricated directly on the cathode side of the bipolar plate. It is worthwhile to mention the structural morphology of STG is determined through the adjustment of the dominant factors including temperature and period [33]. If the Lidenfrost phenomena occur or flooded liquid film is formed at the target surface, the desired porous graphene structure (i.e. STG) could not be constructed. The applied ABM condition to construct STG on the bipolar plate was optimized via our experimental results (Fig. S2). Following this process condition, we could obtain the highly uniform STG structure, as shown in Fig. S3. The detailed information about automatic spray control system (ASCS) is provided in supporting information and previous study [33].

### *TGA and thermal annealing of the STG flow distributor*

As discussed above, additional thermal annealing after the chemical reduction of graphene oxide is the assuring technique to recover the surface properties of the chemically exfoliated graphene, especially the electrical conductivity, to the original properties of pristine graphene. In this study, we varied the temperature of the thermal annealing process to optimize the single cell with STG distributor that can exhibit the best performance. Hence, the TGA was carried out to determine the reasonable temperature condition of thermal annealing (TA Instruments, TGA Q500). The maximum temperature was set to 950 °C, and the temperature increase rate was set as 5 °C/min under the inert gas flow condition. When it comes to the thermal annealing of STG flow distributor, the increase rate of the temperature was set to 5 °C/min, and the flow rate of argon was set as 800 cc/min. When the tubular furnace reaches the target temperature, it is maintained for 90 min at the target temperature. After the annealing process, it is cooled via forced convection of argon flow to room temperature.

### *Preparation of the MEA*

The electrodes of both anode and cathode were prepared by spraying a catalyst ink, which was fabricated through homogeneous mixing Pt/C catalyst with the metal loading of 40 wt% (purchased from Johnson Matthey) and 5 wt% Nafion® ionomer solution, which density is 0.874 g/ml. The weight percentage of Nafion® ionomer with respect to the total weight of the dry mixture (Nafion® + Pt/C) was 23 wt %. After then, deionized water and isopropyl alcohol purchased from Sigma-Aldrich were added to control the viscosity of the catalyst inks. The mixture was ultra-sonicated and sprayed onto the surface of Nafion® 211 membrane on both sides with an active area of 5 $cm^2$ and the Pt-loadings were 0.2 $mg/cm^2$, respectively. The catalyst-coated membrane (CCM) was dried at ambient temperature for more than 12 h to evaporate residual deionized water and isopropyl alcohol. The membrane electrode assembly (MEA) was symmetrically assembled with the Teflon-type gaskets and gas diffusion layers with a microporous layer (GDL, JNTG-30-A3, Korea) on both the anode and cathode side. The layer of the cathode side was covered with STG constructed bipolar plate and that of the anode side was covered with bipolar plate composed of serpentine type channel with a width and rib of 1 mm. The Fig. S5 shows brief information about the single-cell assembly process which includes inlet/outlet direction and applied PEMFC components in this study.

### *PEMFC operation condition*

99.9% pure hydrogen and 99.9% air were used as fuel and oxidant on each anode and cathode side, respectively. The relative humidity (RH) was set as equal to anode and cathode for each experimental case. In this study, we varied the fuel cell operating conditions which are 70 °C of cell temperature

with fully humidified, and 90 °C with near dry-humidity (RH 44%) conditions, respectively. The flow rate of the $H_2$ (150 ml $min^{-1}$) and air (800 ml $min^{-1}$) was continuously maintained to the anode and cathode without back pressure, respectively. As previously reported, applying porous media as a cathode flow distributor has more advantages than at the anode due to its high water removal [34]. And hydrogen oxidation reaction (HOR) at the anode side is much more rapid than the oxygen reduction reaction (ORR) at the cathode side [35]. Based on these previous studies, the flow distributor of the anode was fixed with serpentine flow channel which was made of SUS316L to investigate the effect of the thermal annealed STGs (T-STGs) on the cathode side depending on the annealing temperature more apparently. The detailed PEMFC activation and operation process can be founded in supporting information.

### *EIS analysis*

In order to investigate the losses of the single cell with different T-STG flow distributor, EIS analysis (BioLogic, HCP-803) was conducted for each cell in the same condition with each operating condition. The EIS analysis was carried out with a sine wave amplitude of 5 mV at 0.6 V, and the frequency range was set from 0.1 Hz to 100 kHz [36,37]. The evaluated EIS data was fitted through the Z-View program from Scribner Associates Inc., United States.

## Results & discussion

### *PEMFC operation with T-STG flow distributors and its characterization*

The schematic illustration of the construction process of improved STG flow distributor through thermal annealing process is depicted in Fig. 1. (see detailed fabrication process in the experimental section) Before determining annealing temperature for the constructed STG, TGA was carried out to figure out the thermal decomposition rate of STG according to temperature. As shown in Fig. 2, thermal decomposition of the STG begins near 200 °C and it was rapidly increased around 800 °C. The target temperature conditions for the thermal annealing were set to 300 °C, 400 °C, and 500 °C, based on the assumption that about 30% of mass loss could induce the

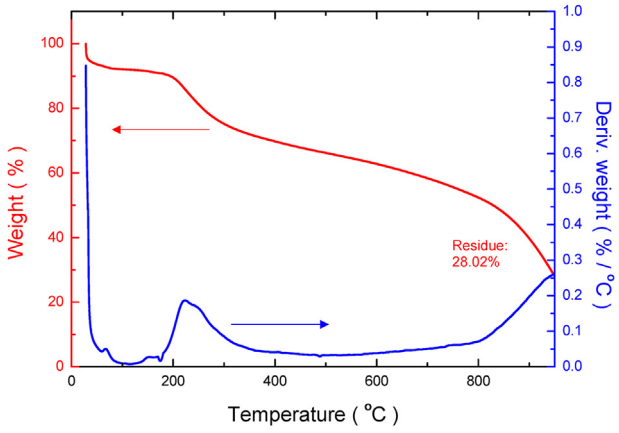


**Fig. 2 – Thermo gravimetric analysis (TGA) result of STG.**

serious structural loss of STG. After the thermal annealing process, the surface morphologies of each STG were observed by using field emission-scanning electron microscopy (JEOL, JSM-7800F) at an acceleration voltage of 10.0 kV to confirm the structural collapse due to the thermal decomposition (Fig. 3). At the high-magnitude SEM images of STGs, it is observed that each STGs showed quite similar morphologies and all of STGs have numerous micro-scale pores ranging in 1~10 μm as shown in Fig. 3. These SEM images indicate that the structural collapse did not occur during the thermal annealing process at each temperature condition. With these numerous pores, the effective removal of generated water in the STG can be expected. As investigated in the previous studies, liquid water discharged from the catalyst layer is gathered at the interface of GDL and the porous flow distributor [5,38]. When the collected water droplet touches the pore structure of the flow distributor, the liquid film spread into the pores via capillary action. And the liquid film filling the pores across the flow distributor is drained by the unused reactant without blocking the pore structures. The maintained dynamic equilibrium leads to the tolerance to flooding in the porous flow distributor. Based on these results, the flow distributors for PEMFC operating were prepared as follows: bare STG, thermally annealed at 300 °C STG flow distributor (T300-STG), thermally annealed at 400 °C STG flow distributor (T400-STG), and thermally annealed at 500 °C STG flow distributor (T500-STG).

Before operating the single cells with T-STG flow distributors, in order to confirm the reproducibility of the STG flow

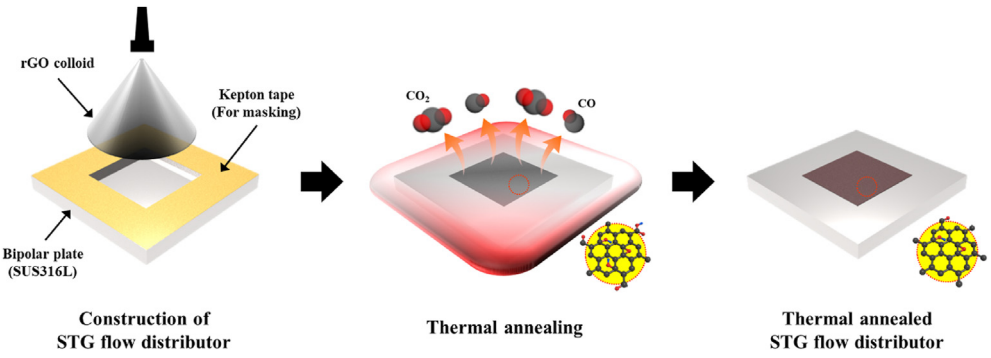


**Fig. 1 – Schematics of construction process of improved STG flow distributor through thermal annealing process.**

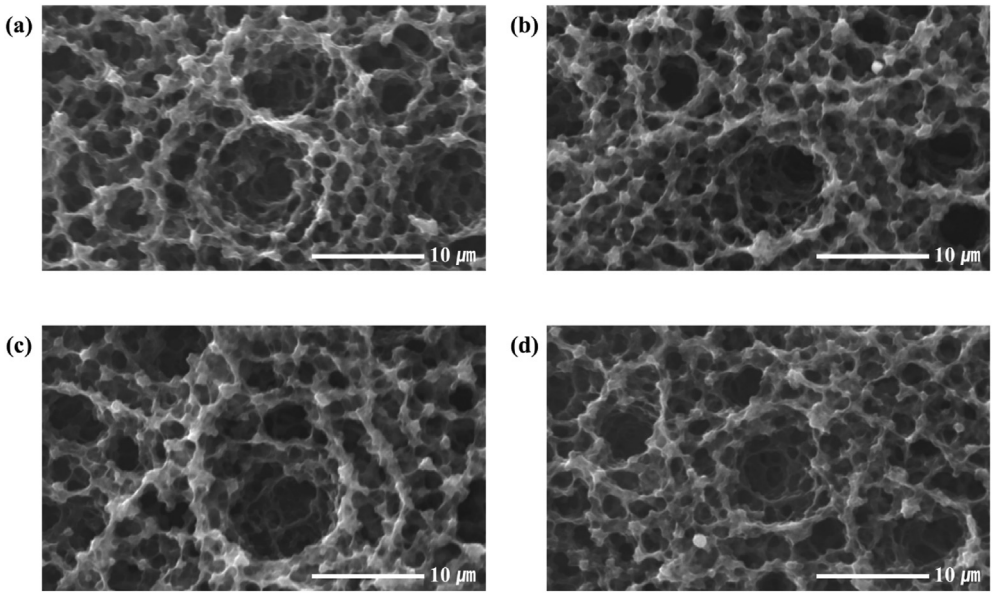


**Fig. 3 – SEM images of (a) bare STG, (b) T300-STG, (c) T400-STG, and (d) T500-STG.**

distributor, we have constructed five bare STG flow distributors respectively, and the performance of fuel cell with each flow distributor was measured in the same operating condition (70 °C and RH 100%). As shown in Fig. S7, the single cells with bare STG flow distributor showed quite similar performance, which confirms reproducibility of the STG flow distributor showed high reproducibility in the aspect of device performance. Afterward, the single cell with each T-STG was assembled and evaluated as shown in Fig. 4(a). In the polarization curves, the remarkable enhancement of each T-STG flow distributor was observed under 70 °C and the fully humidified (RH 100%) condition. The maximum power density of T300-STG flow distributor exhibited 730 mW $cm^{-2}$, which value is ~28% higher than that of the bare STG without annealing (572 mW $cm^{-2}$). Also, clear-cut fuel cell performance enhancement was achieved with T400-STG flow distributor. The PEMFC with T400-STG flow distributor exhibited a maximum power density of 820 mW $cm^{-2}$, which was ~44% higher than that of bare STG flow distributors. However, single cell with T500-STG flow distributor showed the degraded maximum power density (680 mW $cm^{-2}$) compared to that of T400-STG flow distributor.

For further investigation of the exhibited single cell performances with various T-STG flow distributors, the EIS analysis was carried out to estimate each loss of the PEMFC system. Fig. 5(a) shows the EIS measurement results of the operated single cells at 0.6 V. It is noted that the experimental conditions including humidity, cell temperature, and flow rate were fixed corresponding to polarization test conditions. As shown in Fig. 5(a) and Table 1, the single cell systems with various T-STG flow distributors exhibited lowered ohmic resistance ($R_{ohmic}$) than that of single cell with bare STG flow distributor. The T300-STG and T400-STG showed 0.0616 Ω $cm^2$ and 0.0518 Ω $cm^2$, which was lowered than that of the bare

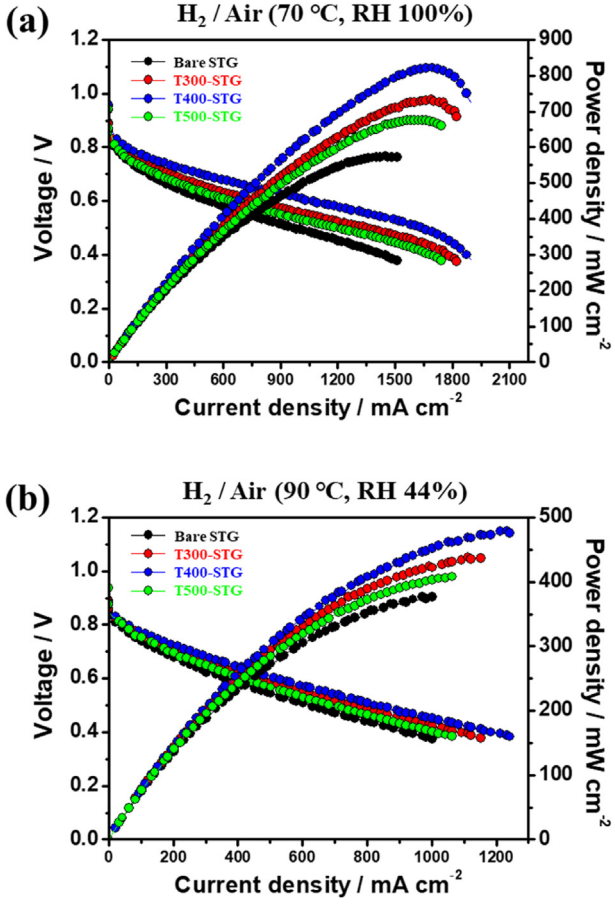


**Fig. 4 – Polarization and power density curves of the STG cases under (a) RH 100% at 70 °C of cell temperature condition and (b) RH 44% at 90 °C of cell temperature condition.**

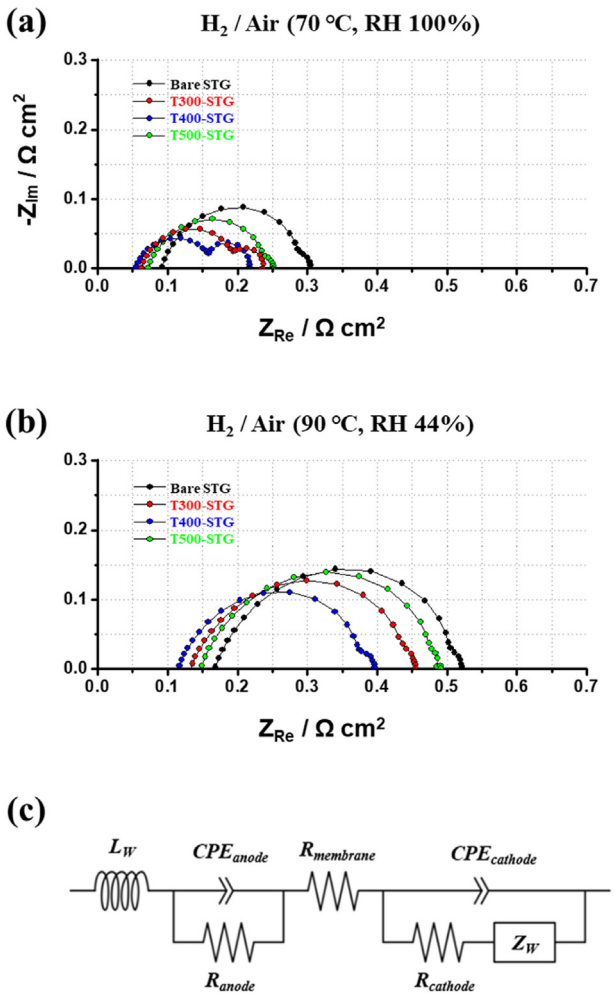


**Fig. 5 – EIS measurement of single cells at 0.6 V under (a) RH 100% at 70 °C of cell temperature condition and (b) RH 44% at 90 °C of cell temperature condition, and (c) Equivalent circuit for the EIS analysis.**

**Table 1 – EIS fitting data.**

| 70 °C, RH 100% | $R_{membrane}$ at 0.6 V [Ω cm$^2$] | $R_{cathode}$ at 0.6 V [Ω cm$^2$] | $Z_{warburg}$ at 0.6 V [Ω cm$^2$] |
|---|---|---|---|
| Bare STG | 0.0831 (–) | 0.1687 (–) | 0.0422 (–) |
| T300-STG | 0.0616 (–25.9%) | 0.1105 (–34.5%) | 0.0503 (19.2%) |
| T400-STG | 0.0518 (–37.7%) | 0.0730 (–56.7%) | 0.0549 (30.1%) |
| T500-STG | 0.0698 (–16.0%) | 0.1424 (–15.6%) | 0.0450 (6.64%) |
| **90 °C, RH 44%** | | | |
| Bare STG | 0.1655 (–) | 0.3182 (–) | 0.0119 (–) |
| T300-STG | 0.1249 (–24.5%) | 0.2461 (–22.7%) | 0.0135 (13.4%) |
| T400-STG | 0.1109 (–33.0%) | 0.1984 (–37.7%) | 0.0149 (25.2%) |
| T500-STG | 0.1374 (–17.0%) | 0.2923 (–8.14%) | 0.0125 (5.04%) |

STG (0.0831 Ω cm$^2$) about ~25.9% and ~37.7%, respectively. As reported in the previous studies, residual oxygen-containing functional groups in the basal plane of rGO sheet can induce the degradation of electrical conductivity [29,33], and the temperature condition of the thermal annealing greatly affects the deoxygenation efficiency of chemically exfoliated graphene [39]. As the annealing temperature is favorable for better deoxygenation of the graphene, the degree of reduction for T400-STG can be increased than that of the T300-STG via efficiently decompose residual oxygen-containing functional groups. And this phenomenon results in lower ohmic resistance than that of the single cell with T300-STG distributor. Nevertheless, in the case of T500-STG flow distributor, the ohmic resistance of single cell was increased in comparison with that of a single cell with T400-STG flow distributor. The result is thought to be caused by the oxidation of the bipolar plate, which was made of SUS316L during the annealing process. Although thermal treatment was carried out at the argon flow condition, there would be residual air and it induced the oxidation of the SUS316L. As shown in Fig. 6, we observed that thermal annealed SUS316L at 500 °C was highly oxidized and degraded than bare SUS316L and the thermal annealed SUS316L at 400 °C. As the STG is a highly porous graphene material, residual air could affect the surface of the bipolar plate without any hinder. This highly oxidized bipolar plate leads to reduced device performance of the single cell with T500-STG via higher ohmic resistance than that of single cell with T400-STG. Based on the fact that the bipolar plate was oxidized during the thermal annealing process as shown in Fig. 6, we measured the electrical resistance to clarify the oxidation effect of the SUS316L plate from the different annealing temperature (Fig. S8). As shown in Fig. S8(a), the total resistance including the SUS316L plate was increased as the annealing temperature increased. The total interfacial contact resistance of the imitated PEMFC with the bare SUS316L was 0.287 Ω cm$^2$, which was sufficiently lower than that of including the thermal annealed SUS316L. The measured total electrical resistances of imitated PEMFC with thermally annealed SUS316L at the temperature of 300 °C, 400 °C, and 500 °C were 0.355, 0.372, and 0.683 Ω cm$^2$, respectively. The electrical resistances slightly increased after thermal annealing under 300 °C and 400 °C, while the electrical resistances significantly increased from the temperature over 500 °C. Especially, SUS plate with an annealing temperature of 600 °C exhibits the highest electrical resistances among the experimental set. The results indicate that the reduced performance of fuel cells with T500-STG comes from the oxidation of the bipolar plate. However, in the view of the STG, which consists of rGO sheets, the higher annealing temperature benefits to remove the oxygen functionalities on the rGO basal plane which induce the decreased electrical resistance [39]. Hence, the favorable annealing temperature of STG flow distributor constructed on SUS plate should be ranged considering both extents of STG property recovery and oxidation of the bipolar plate, and that is why T400-STG exhibits the lowest ohmic resistance among the experimental set in this study. In the aspect of charge transfer resistance, as the previous studies report the properly modified bipolar plates are responsible for reduced ohmic and charge transfer resistance of the PEMFC system [40–42], T-STG flow distributor also is expected to reduce the losses. As shown in Table 1, the charge transfer resistance of T300-STG was 0.1105 Ω cm$^2$ and that of T400-STG was 0.0730 Ω cm$^2$, which were much lower than that of the bare STG flow distributor (0.1687 Ω cm$^2$). Same as the reduced ohmic resistance, the charge transfer resistance ($R_{cathode}$) of each T-STGs is effectively lowered through the thermal annealing process. When it comes to the

mass transport resistance (Warburg impedance, $Z_W$), a different tendency was observed from the ohmic and charge transfer resistance. Based on the fact that the non-annealed bipolar plate showed lower Warburg impedance than that of all the annealed bipolar plate, thermal annealing seems to be responsible for increasing the Warburg impedance. This phenomenon can be analyzed from the perspective of wettability change of the bipolar plate. Previous reports demonstrated that the hydrophobic surface property of bipolar plate is favorable to reduce the mass transport loss of fuel cell systems [3,5,6]. In order to observe the thermal annealing effect on the wettability change of bipolar plate surface, the contact angle of bare and thermally annealed bipolar plates was measured at room temperature and humidity through dispensing 10 μl of the deionized water droplet (FEMTOBIOMED, SmartDrop) on the surface. As shown in Fig. 7, the hydrophilicity of bipolar plate was increased after the thermal annealing treatment. These results indicate that the increased hydrophilicity of the bipolar plate during thermal annealing process would cause the higher mass transport loss of single cell. The EIS analysis demonstrates that ohmic/charge transfer resistances are decreased and mass transport resistance is increased during the thermal annealing process, which means thermal annealing should be conducted at the proper temperature considering the change of three resistances. Although the mass transport resistance was increased after the thermal annealing process, it is worthwhile to mention the kinetic resistance ($R_{cathode} + Z_W$) was reduced for all the T-STG compared to bare STG, which indicates that the positive effect of thermal annealing on device performance was obtained apparently.

In order to verify if the T-STG is still effective for enhancing performance in low humidified operating condition, the single cells are evaluated under 90 °C and RH 44% condition. The measured maximum power densities of T300-STG, T400-STG, and T500-STG flow distributor were about 431 mW $cm^{-2}$, 479 mW $cm^{-2}$ and 409 mW $cm^{-2}$, respectively, which was higher than that of bare STG case (379 mW $cm^{-2}$). Notably, single cell with T400-STG flow distributor showed the highest maximum power density, which is ~26.4% higher compared to bare STG flow distributor. As the same procedures, these results were verified via EIS analysis. As shown in Fig. 5(b), the lowest ohmic resistance was observed in the 400T-STG flow

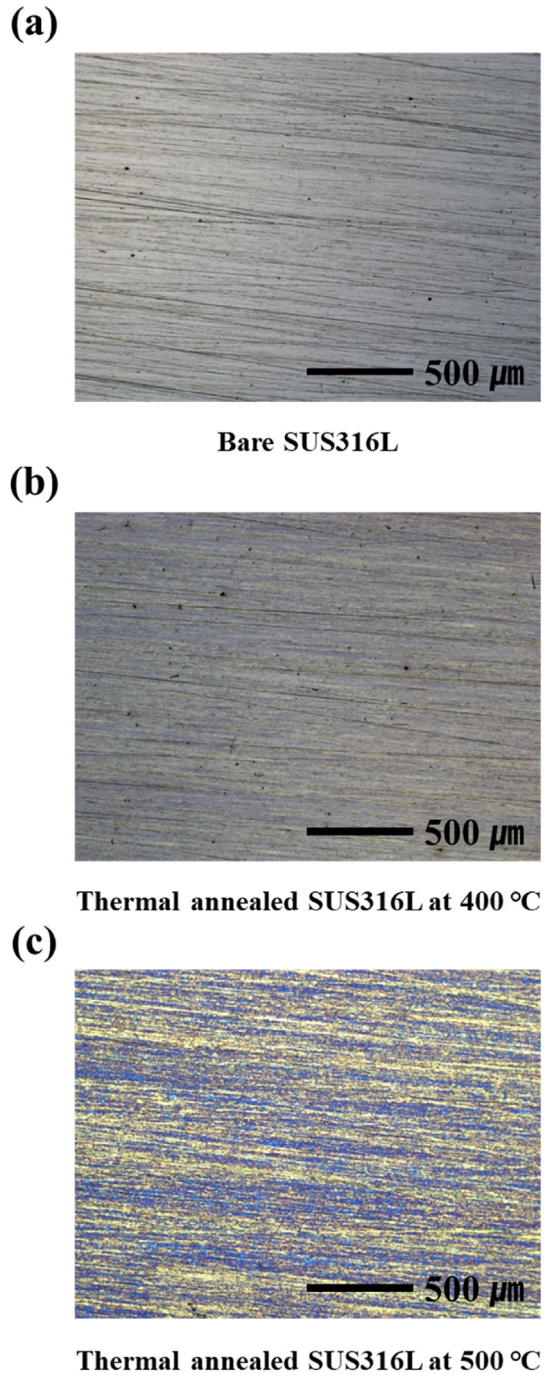


**Fig. 6 – Optical microscope images of the (a) bare SUS316L, (b) thermal annealed SUS316L at 400 °C, and (c) thermal annealed SUS316L at 500 °C.**

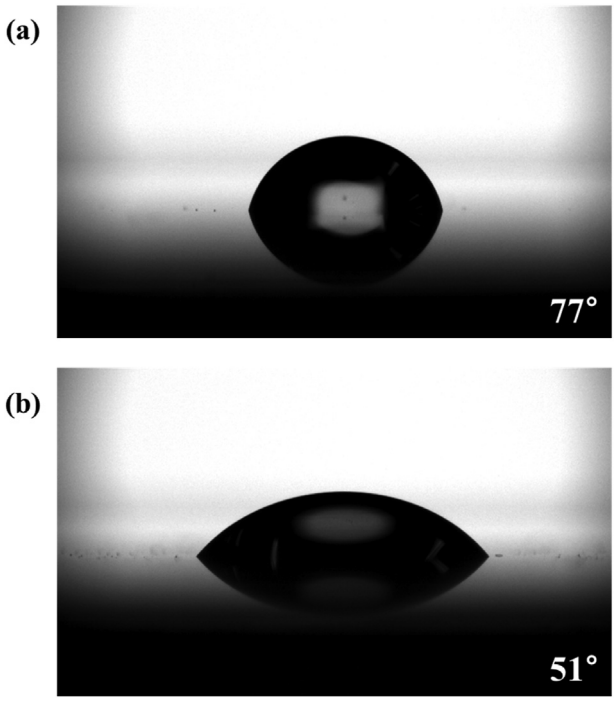


**Fig. 7 – Contact angle of (a) bare SUS316L, (b) thermal annealed SUS316L at 400 °C.**

distributor, which is ~33.0% lowered value than that of bare STG flow distributor. Furthermore, the values of ohmic resistance and charge transfer resistance of the samples are in the same order as that of fully humidified condition, which shows a duplicative tendency with previous EIS measurement results. When it comes to mass transport resistance, all of the single cells with T-STG also exhibited the increased mass transport resistance compared to that of bare STG. As discussed above, this result was caused by the changed wettability of bipolar plate during thermal annealing process. It is noted that the tendency of comparative change of three resistances in the low humidified condition is quite comparable with that in the previous PEMFC operating condition. The detailed values of each resistance at the different PEMFC operating condition are provided in Table 1. As the single cell with T400-STG flow distributor exhibited the highest performance, further XPS analysis of the bare and T400-STG was carried out to verify the effect of the thermal annealing to the STG. With XPS analysis, the presence of residual oxide functional groups (C–O and C=O) in both STG and T400-STG were confirmed (Fig. 8(a)). And in the analysis of the atomic composition of STG and T400-STG derived from XPS survey, meaningful change from the effect of the thermal annealing process was observed. The carbon composition of STG increased from 80.8% to 87.7%, while the oxygen composition reduced from 13.9% to 5.4% after thermal annealing as shown in Fig. 8(b). Furthermore, as recently published, the T400-STG exhibited increased electrical conductivity than that of bare STG in the previous study [33]. Referring to the discussed electrochemical analysis and performance of single cell with various T-STG flow distributors, we report that thermal annealing of STG flow distributor is the promising technique to achieve high-performance PEMFC, with possession of advantages including low-cost, facile procedures, and direct 3D structuring without using any backbone structure. And based on the experimental results, the annealing temperature around 400 °C seems to be the optimized temperature for the annealing process of STG flow distributor with the SUS316L bipolar plate.

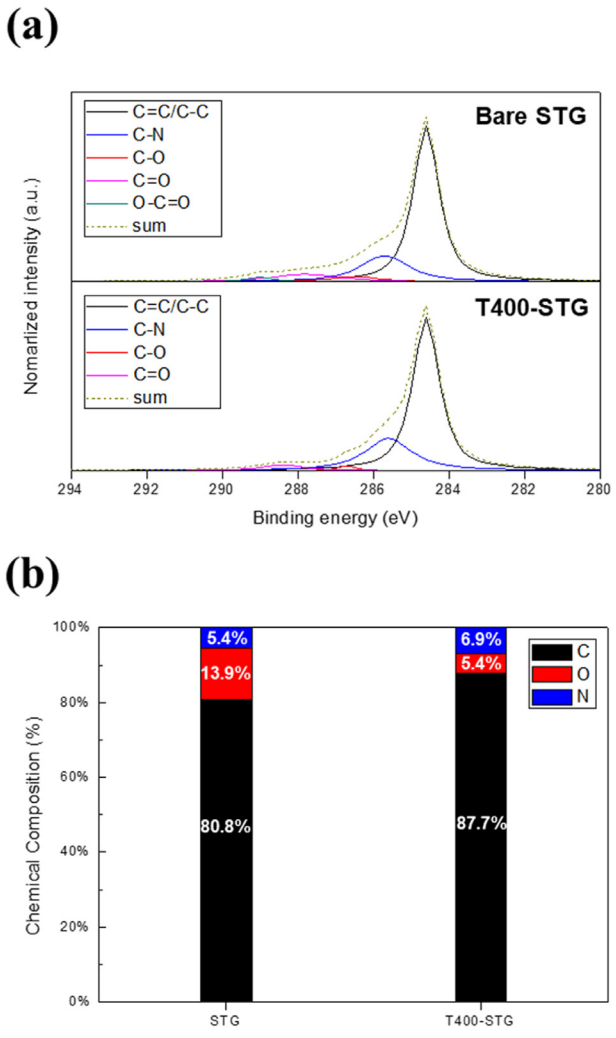


**Fig. 8 – (a) XPS C1s spectra of STGs and (b) chemical composition of STGs derived from XPS survey.**

## Conclusions

Herein, the advanced STG flow distributor is developed via the thermal annealing process and optimized condition for the annealing temperature was investigated. The thermal annealing process can induce the recovery of conductivity of the STG flow distributor, which directly impacts single-cell performance. The porous STG flow distributor on the SUS316L bipolar plate via advanced boiling method was successfully constructed, and the STG flow distributor was thermally treated with an annealing temperature of 300 °C, 400 °C, and 500 °C. The physicochemical characteristics of the thermally annealed STG flow distributors were investigated through SEM analysis, XPS analysis, EIS analysis, and TGA. Based on these analyses, the conclusions of this study are as follows.

1. The thermal annealing process is the assuring technique to enhance the single cell performance with STG flow distributor. The PEMFC with thermally annealed STG flow distributor exhibited dramatic fuel cell performance enhancement than that of bare STG flow distributor. The optimized heat-treatment condition was observed as 400 °C for the STG flow distributor, which was constructed on the SUS316L bipolar plate.*
2. The enhanced single-cell performance with thermally annealed STG flow distributor came from the recovery of conductivity of the STG, which was made of chemically exfoliated graphene. After the thermal annealing process, the modified properties of bipolar plate lead to the lowered ohmic and charge transfer resistance in single cell system with T-STG flow distributors.
3. All of the single cells with T-STG showed higher mass transport resistance than that of bare STG. The result was caused by an increase in the hydrophilicity of bipolar plates (SUS316L) during the thermal annealing process. These results indicate that thermal annealing process should be conducted at the proper range of temperature.

Based on the results, the improved STG flow distributors via thermal annealing process at the proper temperature is assuring technique for realizing high performance 3D porous flow distributor in PEMFC. This facile and simple method for

realizing direct 3D porous structuring without using any backbone structure while assuring high conductivity and chemical resistance can be broadly used in energy storage and conversion devices including fuel cell, battery, and supercapacitor.

## Declaration of competing interest

The authors declare that they have no known competing financial interests or personal relationships that could have appeared to influence the work reported in this paper.

## Acknowledgements

This work was supported by Korea Electric Power Corporation (grant number: R19XO01-29), and by the National Research Foundation of Korea (grant number: 2019R1C1C1006392).

## Appendix A. Supplementary data

Supplementary data to this article can be found online at https://doi.org/10.1016/j.ijhydene.2021.08.210.

## REFERENCES

[1] Maricle DL, Nagle DC. Carbon foam fuel cell components. Google Patents; 1978.
[2] Kumar A, Reddy RG. Materials and design development for bipolar/end plates in fuel cells. J Power Sources 2004;129:62–7.
[3] Tseng C-J, Tsai BT, Liu Z-S, Cheng T-C, Chang W-C, Lo S-K. A PEM fuel cell with metal foam as flow distributor. Energy Convers Manag 2012;62:14–21.
[4] Lee Y-H, Li S-M, Tseng C-J, Su C-Y, Lin S-C, Jhuang J-W. Graphene as corrosion protection for metal foam flow distributor in proton exchange membrane fuel cells. Int J Hydrogen Energy 2017;42:22201–7.
[5] Park JE, Lim J, Kim S, Choi I, Ahn C-Y, Hwang W, et al. Enhancement of mass transport in fuel cells using three-dimensional graphene foam as flow field. Electrochim Acta 2018;265:488–96.
[6] Jang S, Park H-Y, Jung J, Lee J, Park H-Y, Jang JH, et al. Enhanced water management of three-dimensional graphene-Ni foam with patterned wettability in a polymer electrolyte membrane fuel cell. ACS Sustainable Chem Eng 2019;7:15487–94.
[7] Park JE, Lim J, Lim MS, Kim S, Kim O-H, Lee DW, et al. Gas diffusion layer/flow-field unified membrane-electrode assembly in fuel cell using graphene foam. Electrochim Acta 2019;323:134808.
[8] Ramos-Alvarado B, Hernandez-Guerrero A, Juarez-Robles D, Li P. Numerical investigation of the performance of symmetric flow distributors as flow channels for PEM fuel cells. Int J Hydrogen Energy 2012;37:436–48.
[9] André J, Antoni L, Petit J-P. Corrosion resistance of stainless steel bipolar plates in a PEFC environment: a comprehensive study. Int J Hydrogen Energy 2010;35:3684–97.
[10] Joseph S, McClure JC, Chianelli R, Pich P, Sebastian P. Conducting polymer-coated stainless steel bipolar plates for proton exchange membrane fuel cells (PEMFC). Int J Hydrogen Energy 2005;30:1339–44.
[11] Pozio A, Silva R, De Francesco M, Giorgi L. Nafion degradation in PEFCs from end plate iron contamination. Electrochim Acta 2003;48:1543–9.
[12] Wang H, Sweikart MA, Turner JA. Stainless steel as bipolar plate material for polymer electrolyte membrane fuel cells. J Power Sources 2003;115:243–51.
[13] Wind J, Späh R, Kaiser W, Böhm G. Metallic bipolar plates for PEM fuel cells. J Power Sources 2002;105:256–60.
[14] Compton OC, Nguyen ST. Graphene oxide, highly reduced graphene oxide, and graphene: versatile building blocks for carbon-based materials. Small 2010;6:711–23.
[15] Geim AK, Novoselov KS. The rise of graphene. In: Nanoscience and technology: a collection of reviews from nature journals. World Scientific; 2010. p. 11–9.
[16] Novoselov KS, Fal V, Colombo L, Gellert P, Schwab M, Kim K. A roadmap for graphene. Nature 2012;490:192–200.
[17] Novoselov KS, Jiang Z, Zhang Y, Morozov S, Stormer HL, Zeitler U, et al. Room-temperature quantum Hall effect in graphene. Science 2007;315:1379.
[18] Shi J-N, Ger M-D, Liu Y-M, Fan Y-C, Wen N-T, Lin C-K, et al. Improving the thermal conductivity and shape-stabilization of phase change materials using nanographite additives. Carbon 2013;51:365–72.
[19] Stoller MD, Park S, Zhu Y, An J, Ruoff RS. Graphene-based ultracapacitors. Nano Lett 2008;8:3498–502.
[20] Böhm S. Graphene against corrosion. Nat Nanotechnol 2014;9:741–2.
[21] Sim Y, Kwak J, Kim S-Y, Jo Y, Kim S, Kim SY, et al. Formation of 3D graphene–Ni foam heterostructures with enhanced performance and durability for bipolar plates in a polymer electrolyte membrane fuel cell. J Mater Chem 2018;6:1504–12.
[22] Pu N-W, Shi G-N, Liu Y-M, Sun X, Chang J-K, Sun C-L, et al. Graphene grown on stainless steel as a high-performance and ecofriendly anti-corrosion coating for polymer electrolyte membrane fuel cell bipolar plates. J Power Sources 2015;282:248–56.
[23] Kakati BK, Ghosh A, Verma A. Efficient composite bipolar plate reinforced with carbon fiber and graphene for proton exchange membrane fuel cell. Int J Hydrogen Energy 2013;38:9362–9.
[24] Cao X, Shi Y, Shi W, Lu G, Huang X, Yan Q, et al. Preparation of novel 3D graphene networks for supercapacitor applications. Small 2011;7:3163–8.
[25] Lee YH, Noh S, Lee J-H, Chun S-H, Cha SW, Chang I. Durable graphene-coated bipolar plates for polymer electrolyte fuel cells. Int J Hydrogen Energy 2017;42:27350–3.
[26] Lee GW, Shim GH, Kim JM, Seol C, Kim JH, Kim SM, et al. Two/three-dimensional reduced graphene oxide coating for porous flow distributor in polymer electrolyte membrane fuel cell. Int J Hydrogen Energy 2020;45:12972–81.
[27] Cançado LG, Da Silva MG, Ferreira EHM, Hof F, Kampioti K, Huang K, et al. Disentangling contributions of point and line defects in the Raman spectra of graphene-related materials. 2D Mater 2017;4:25039.
[28] Dong L, Yang J, Chhowalla M, Loh KP. Synthesis and reduction of large sized graphene oxide sheets. Chem Soc Rev 2017;46:7306–16.
[29] Stankovich S, Dikin DA, Piner RD, Kohlhaas KA, Kleinhammes A, Jia Y, et al. Synthesis of graphene-based nanosheets via chemical reduction of exfoliated graphite oxide. Carbon 2007;45:1558–65.
[30] Gao X, Jang J, Nagase S. Hydrazine and thermal reduction of graphene oxide: reaction mechanisms, product structures, and reaction design. J Phys Chem C 2010;114:832–42.

[31] Renteria JD, Ramirez S, Malekpour H, Alonso B, Centeno A, Zurutuza A, et al. Strongly anisotropic thermal conductivity of free-standing reduced graphene oxide films annealed at high temperature. Adv Funct Mater 2015;25:4664–72.
[32] Marcano DC, Kosynkin DV, Berlin JM, Sinitskii A, Sun Z, Slesarev A, et al. Improved synthesis of graphene oxide. ACS Nano 2010;4:4806–14.
[33] Kim JH, Kim JM, Lee GW, Shim GH, Lim ST, Kim KM, et al. Advanced boiling–A scalable strategy for self-assembled three-dimensional graphene. ACS Nano 2021;15:2839–48.
[34] Shudo T, Suzuki K. Performance improvement in direct methanol fuel cells using a highly porous corrosion-resisting stainless steel flow field. Int J Hydrogen Energy 2008;33:2850–6.
[35] Song C, Tang Y, Zhang JL, Zhang J, Wang H, Shen J, et al. PEM fuel cell reaction kinetics in the temperature range of 23–120 C. Electrochim Acta 2007;52:2552–61.
[36] Wagner N. Characterization of membrane electrode assemblies in polymer electrolyte fuel cells using ac impedance spectroscopy. J Appl Electrochem 2002;32:859–63.
[37] Yuan X, Wang H, Sun JC, Zhang J. AC impedance technique in PEM fuel cell diagnosis—a review. Int J Hydrogen Energy 2007;32:4365–80.
[38] Tabe Y, Nasu T, Morioka S, Chikahisa T. Performance characteristics and internal phenomena of polymer electrolyte membrane fuel cell with porous flow field. J Power Sources 2013;238:21–8.
[39] Yang D, Velamakanni A, Bozoklu G, Park S, Stoller M, Piner RD, et al. Chemical analysis of graphene oxide films after heat and chemical treatments by X-ray photoelectron and Micro-Raman spectroscopy. Carbon 2009;47:145–52.
[40] Cho E, Jeon U-S, Ha H, Hong S-A, Oh I-H. Characteristics of composite bipolar plates for polymer electrolyte membrane fuel cells. J Power Sources 2004;125:178–82.
[41] Cho E, Jeon U-S, Hong S-A, Oh I-H, Kang S-G. Performance of a 1 kW-class PEMFC stack using TiN-coated 316 stainless steel bipolar plates. J Power Sources 2005;142:177–83.
[42] Li W, Jing S, Wang S, Wang C, Xie X. Experimental investigation of expanded graphite/phenolic resin composite bipolar plate. Int J Hydrogen Energy 2016;41:16240–6.